One or more of the Following Statements may affect this Document

- This document has been reproduced from the best copy furnished by the organizational source. It is being released in the interest of making available as much information as possible.

- This document may contain data, which exceeds the sheet parameters. It was furnished in this condition by the organizational source and is the best copy available.

- This document may contain tone-on-tone or color graphs, charts and/or pictures, which have been reproduced in black and white.

- This document is paginated as submitted by the original source.

- Portions of this document are not fully legible due to the historical nature of some of the material. However, it is the best reproduction available from the original submission.

NASA TM X-56041

SEMIEMPIRICAL AIRFRAME NOISE PREDICTION MODEL AND EVALUATION WITH FLIGHT DATA

Alan S. Hersh, Frank W. Burcham, Jr.,
Terrill W. Putnam, and Paul L. Lasagna

December 1976

NASA high-number Technical Memorandums are issued to provide rapid transmittal of technical information from the researcher to the user. As such, they are not subject to the usual NASA review process.

NASA Dryden Flight Research Center
Edwards, California 93523

1. Report No.	2. Government Accession No.	3. Recipient's Catalog No.
NASA TM X-56041		

4. Title and Subtitle	5. Report Date
SEMIEMPIRICAL AIRFRAME NOISE PREDICTION MODEL AND EVALUATION WITH FLIGHT DATA	December 1976
	6. Performing Organization Code H-951
7. Author(s)	8. Performing Organization Report No.
Alan S. Hersh, Frank W. Burcham, Jr., Terrill W. Putnam, and Paul L. Lasagna	
	10. Work Unit No. 505-11-26
9. Performing Organization Name and Address	11. Contract or Grant No.
Hersh Acoustical Engineering, 9545 Cozycroft Avenue, Chatsworth, California 91311 — NASA Dryden Flight Research Center, P.O. Box 273, Edwards, California 93523	NAS4-2250
	13. Type of Report and Period Covered Technical Memorandum
12. Sponsoring Agency Name and Address	14. Sponsoring Agency Code
National Aeronautics and Space Administration, Washington, D.C. 20546	

15. Supplementary Notes

Some of the information presented herein was previously included in the paper "Semi-Empirical Airframe Noise Prediction Model", presented by the authors at the AIAA 3rd Aero-Acoustics Conference, Palo Alto, California, July 20 to 22, 1976.

16. Abstract

A semiempirical maximum overall sound pressure level (OASPL) airframe noise model was derived. The noise radiated from aircraft wings and flaps was modeled by using the trailing-edge diffracted quadrupole sound theory derived by Ffowcs Williams and Hall. The noise radiated from the landing gear was modeled by using the acoustic dipole sound theory derived by Curle. The model was successfully correlated with maximum OASPL flyover noise measurements obtained at the NASA Dryden Flight Research Center for three jet aircraft—the Lockheed JetStar, the Convair 990, and the Boeing 747 aircraft. The model was also used to correlate and interpret one-third octave band sound pressure level flyover data.

17. Key Words (Suggested by Author(s))	18. Distribution Statement
Airframe noise Nonpropulsive noise	Unclassified—Unlimited STAR Category: 71

19. Security Classif. (of this report)	20. Security Classif. (of this page)	21. No. of Pages	22. Price*
Unclassified	Unclassified	35	

*For sale by the National Technical Information Service, Springfield, Virginia 22161

SEMIEMPIRICAL AIRFRAME NOISE PREDICTION MODEL AND EVALUATION WITH FLIGHT DATA

Alan S. Hersh
Hersh Acoustical Engineering

and

Frank W. Burcham, Jr., Terrill W. Putnam, and Paul L. Lasagna
NASA Dryden Flight Research Center

INTRODUCTION

There is serious and legitimate concern in both government and industry that airframe (nonpropulsive) noise may prevent the achievement of even the upper limits of the 1981 aircraft noise reduction goals set in the 1969-70 DOT/NASA CARD Study (ref. 1). The level of noise produced just by the passage of an airplane through the air, especially in the landing configuration, may be only a few decibels below the level of noise radiated from the engines. It is clear that a need exists to develop a prediction model for the noise generated by the airframe in order to establish realistic aircraft noise reduction goals. The purpose of this report is to present the results of a semiempirical airframe noise prediction model that has successfully correlated the maximum overall sound pressure levels (OASPL) radiated from three aircraft—the Lockheed JetStar, the Convair 990, and the Boeing 747 aircraft. The model is also used to correlate and interpret one-third octave band sound pressure level (OBSPL) data.

SYMBOLS

A_c	dipole correlation area, m^2
A_g	landing gear area, m^2
a	speed of sound, m/sec
b	wingspan, m

C_D	drag coefficient
C_{Dg}	drag coefficient of gear
C_{Dw}	drag coefficient of wing
C_{D_0}	value of C_D at $C_L = 0$
C_L	lift coefficient
C_W	$= W/qS_w$
$\bar{c}$	wing mean aerodynamic chord, m
D	landing gear diameter (fig. 3), m
$D(\mu,\mu_s,\beta)$	directivity factor
D_{ch}	characteristic dimension, m
F	dipole strength
f	frequency, Hz
f_{st}	peak Strouhal frequency, Hz
K	acoustic wave number, ω/a, Hz-sec/m
K_g	acoustic constant for gear
K_w	acoustic constant for wing
K_{wf}	acoustic constant for wing and flaps
K_1,K_2	constants for drag polar
L	landing gear length (fig. 3), m
M	Mach number
OASPL	overall sound pressure level, dB
OBCF	octave band center frequency, Hz

OBSPL	octave band sound pressure level, dB
P	root mean square sound pressure, Pa
$\overline{P_{ref}^2}$	reference mean square sound pressure, 20μPa
P_w	$= \rho U^{2.4} \sqrt{\frac{C_{Dw} S_w \cos^2 \psi}{aR^2 \ (c/\nu)^{0.2}}}$
$\overline{p^2}$	average mean square sound pressure, Pa^2
q	dynamic pressure, N/m^2
R, θ, φ	spherical coordinate (fig. 2)
r_0	radius of eddy, m
S_c	Strouhal number for cylinder
S_w	wing area, m^2
t	time, sec
U	aircraft speed, m/sec
V	volume, m^3
W	weight of aircraft, kg
x,y,z	Cartesian coordinates in space (fig. 4)
α	turbulence intensity
γ	glide slope angle, deg
ΔC_{Dg}	incremental drag coefficient due to landing gear
δ	boundary layer thickness, m
λ	wavelength, m
μ, μ_s, β	directivity angles for dipole sources (fig. 4)
ν	kinematic viscosity, m^2/sec
ρ	air density, kg/m^3

τ	mean wing thickness, m
ψ	wing or flat plate sweep angle, deg
ω	angular frequency, Hz

Subscripts:

f	flap
g	gear
max	maximum
w	wing

DERIVATION OF MODEL EQUATION

The major structural elements that generate airframe noise are the wings (including leading-edge devices and trailing-edge flaps), the landing gear, the wheel well cavities, and the vertical and horizontal tails. Sketches of these elements are shown in figure 1. Curle has shown that whenever surfaces are immersed in turbulent flow, the noise radiated from the distributed acoustic volume quadrupoles is supplemented by noise from other sources, the most important of which is the surface distribution of acoustic dipole sources (ref. 2). Ffowcs Williams and Hall argue that in the case of a semi-infinite half plane containing sharp edges, the edges scatter the quadrupole acoustic sources (ref. 3). They show that the scattered sound field (proportional to aircraft speed, U^5) is more powerful for low speeds than either the direct turbulent quadrupole sound field (ref. 4), which is proportional to U^8, or the surface dipole field of the Curle type (which is proportional to U^6).

In the derivation of the model, the dominant airframe noise sources are assumed to consist of trailing-edge diffracted quadrupole sound of the Ffowcs Williams and Hall type, which is generated principally at the wing and flap trailing edges, and point dipole sources of the Curle type, which are distributed along the landing gear structure. These assumptions are based upon the data reported in references 5 to 7.

In reference 5, Fink conducted tests to measure the noise radiated from surfaces immersed in flow. The measurements showed that the radiated sound varied with velocity to the fifth power (U^5) and the turbulence intensity to the second power (α^2), supporting the theory of Ffowcs Williams and Hall. Putnam, Lasagna, and White analyzed a wide range of airframe noise flyover measurements (ref. 7) and demonstrated correlation to U^5 for aircraft flying in the clean (flaps retracted, landing gear up) configuration. Their measurements also showed significant increases in radiated noise with the deployment of the landing gear.

Trailing-Edge Noise

As derived, the trailing-edge diffraction theory of Ffowcs Williams and Hall applies only to semi-infinite surfaces. It is reasonable to assume that their theory also applies to surfaces of finite size (large wings, for example), provided that $\lambda << \bar{c}$, where λ is the sound wavelength of interest and $\bar{c}$ is the characteristic surface length (that is, wing mean aerodynamic chord). The assumption is that the leading and trailing edges are acoustically isolated if they are separated by many wavelengths. In a recent study, Healy showed that the wing mean aerodynamic chord lengths of most commercial jet aircraft are three to four times the radiated peak acoustic wavelength (ref. 8). By analyzing several kinds of airframe flyover spectral noise data, he predicted that the maximum one-third OBSPL would occur at a frequency, f_{max}, given by the following equation:

$$f_{max} \approx 1.3U/\tau$$

where U is airspeed and τ is mean wing thickness. Healy stated that $\tau = 0.11\bar{c}$ is a reasonable value for most current transport aircraft. By substituting this value for τ in the above equation, the ratio $\lambda_{max}/\bar{c}$ for the peak in the spectra can be calculated as follows:

$$\lambda_{max}/\bar{c} = a/f_{max}\bar{c} = \tau a/1.3U\bar{c} \approx 0.085/M$$

Assuming a Mach number of approximately 0.3 as a representative approach speed for large commercial jet aircraft, $\lambda_{max}/\bar{c} \approx 0.3$. Thus, the mean aerodynamic chord of most commercial jet transports is roughly three times the wavelength at the Strouhal peak frequency, supporting the use of the Ffowcs Williams and Hall theory.

This theory predicts that the presence of a trailing edge in an infinite half plane immersed in turbulent flow greatly increases the noise generated by the fluid at low Mach numbers. Using Lighthill's quadrupole sound theory, Ffowcs Williams and Hall solved for the noise due to the generation and scattering of sound from coherent eddies near the trailing edge of an infinite half plane. By replacing the flow over the plate edge with an equivalent known acoustic source distribution and solving for the appropriate Green's function that satisfied the condition of infinite acoustic impedance at the plate surface, Ffowcs Williams and Hall sought solutions for the cases in which the acoustic sources were near the edge ($Kr_0 << 1$, where K is the acoustic wave number, ω/a, and r_0 is the radius of the eddy) and far from the edge ($Kr_0 >> 1$) in terms of the ratio of eddy diameter to acoustic wavelength. Very near the edge, they found approximate solutions in terms of inverse fractional powers of Kr_0, the largest being $(Kr_0)^{-3/2}$, the next $(Kr_0)^{-1/2}$, and so forth. Their analysis showed that only those eddies that satisfied $Kr_0 << 1$ were affected significantly by the edge and that the sound intensity was greatly amplified by the term $(Kr_0)^{-3/2}$.

They derived the following expression for the radiated mean square sound pressure:

$$\overline{p^2} \approx \frac{\rho^2 U^4 \alpha^2 V^2 K^4 \cos^2(\theta/2) \sin\phi \cos^2\psi}{(Kr_0)^3 R^2} \qquad (1)$$

where V is the eddy volume, ψ is the flat plate sweep angle, R is the distance between an observer and the eddy, α is the eddy turbulence intensity, and θ and φ are the directivity angles in the planes perpendicular to and parallel to the plate, respectively (fig. 2). If it is assumed that the frequency characterizing the eddy is approximately equal to U/δ, so that $K \quad U/\delta a$, and that a typical eddy with radius δ is roughly spherical, so that $r_0 \quad \delta$, then $V \quad \delta^3$ and equation (1) can be reduced to the following equation:

$$\overline{p^2} \approx \frac{\rho^2 U^5 \alpha^2 \delta^2 \cos^2(\theta/2) \sin\phi \cos^2\psi}{aR^2} \qquad (2)$$

Ffowcs Williams and Hall concluded that the scattered sound due to the diffracting edge is proportional to the fifth power of the free-stream velocity. When $Kr_0 >> 1$, the presence of the edge is not important and the sound level follows the familiar U^8 power law.

The derivation of equation (2) assumed that the volume of a single eddy was proportional to δ^3, that the eddy was close enough to the trailing edge so that $K\delta << 1$, and that the maximum sound pressure level occurred at a frequency, f_{max}, proportional to U/δ. Equation (2) represents the sound radiated from a single eddy. To compute the sound radiated from all eddies, equation (2) must be multiplied by the number of coherent eddies distributed along the edges of all lifting surfaces. On the wing, where most of the edge noise is believed to originate, the number of coherent eddies must be related to b/δ, where b is the wingspan. Multiplying equation (2) by the ratio b/δ yields the following equation for an average sound pressure level from the wing:

$$\overline{p_w^2} \approx \frac{\rho^2 U^5 \alpha^2 \delta b \cos^2(\theta/2) \sin\phi \cos^2\psi}{aR^2} \qquad (3)$$

Equation (3) can be cast in a more convenient form by relating δ, the boundary layer thickness at the trailing edge, to wing drag by using the following relationship from reference 9:

$$\delta \approx C_{D_w} \bar{c} \qquad (4)$$

where C_{Dw} is the corresponding wing drag coefficient. Substituting equation (4) into equation (3) yields the following expression:

$$\overline{P_w^2} \approx \frac{\rho^2 U^5 \alpha^2 S_w C_{Dw} \cos^2(\theta/2) \sin\phi \cos^2\psi}{aR^2} \tag{5}$$

where S_w is the wing area, $b\bar{c}$. The quantities α^2 and C_{Dw} represent wing average values. As Powell suggested (ref. 10), equation (5) can be simplified still further by using the following approximation for α^2:

$$\alpha^2 \approx (U\bar{c}/\nu)^{-0.2} \tag{6}$$

This equation follows from the classical one-seventh power law for a turbulent boundary layer velocity profile. Equation (6) is strictly correct only for isotropic turbulent flow, so it constitutes only an approximation when it is applied to a turbulent boundary layer. Substituting equation (6) into equation (5) yields the following equation:

$$\overline{P_w^2} \approx \frac{\rho^2 U^5 C_{Dw} S_w \cos^2(\theta/2) \sin\phi \cos^2\psi}{aR^2 (U\bar{c}/\nu)^{0.2}} \tag{7}$$

In terms of the maximum overall sound pressure level from the wing, $OASPL_w$, equation (7) is written as follows:

$$OASPL_w = 10 \log\left[\frac{K_w C_{Dw} \rho^2 U^{4.8} S_w \cos^2(\theta/2) \sin\phi \cos^2\psi}{\overline{P_{ref}^2} aR^2 (\bar{c}/\nu)^{0.2}}\right] \tag{8}$$

where $\overline{P_{ref}^2}$ is the reference mean square sound pressure, 20 micropascals. For the flaps-down configuration, K_{wf} can be substituted for K_w. The constants K_w and K_{wf} represent the average of the variation of the edge-scattering noise along the aircraft wing (the aircraft operating in the clean configuration) and wing with flaps extended, respectively. Equation (8) shows that the radiated sound pressure from the aircraft wing is linearly proportional to the drag coefficient C_{Dw} and not to the third power of the drag coefficient, as predicted by Revell (ref. 11).

Landing Gear Noise

A typical landing gear consists of various structures, such as supporting struts, wheels, and doors. To create a simplified model of the structure, the landing gear is divided into two highly idealized parts, a single cylindrical strut and a cylindrical body representing the wheels. These structures are shown schematically in figures 3(a) and 3(b).

Noise radiated from a cylinder is assumed to be generated by an array of independent acoustic point dipoles distributed along the surface of the cylinder. Point dipoles were assumed because for most aircraft $\lambda >> D$, where D is the diameter of the cylinder and λ is the wavelength of tne landing gear noise near the frequency of its spectral maximum.

From classical acoustics, the sound pressure radiated from a point dipole can be represented as follows:

$$\overline{p^2} \approx \frac{1}{a^2 R^2} \overline{\left(\frac{\partial F}{\partial t}\right)^2} D(\mu, \mu_s, \beta) \tag{9}$$

where F is the dipole strength and $D(\mu,\mu_s,\beta)$ is a nondimensional sound directivity factor. Reference 12 derived the following general expression for $D(\mu,\mu_s,\beta)$:

$$D(\mu,\mu_s,\beta) = \cos^2 \mu_s \cos^2 \mu + \sin^2 \mu_s \sin^2 \mu \cos^2 \beta + \sin \mu_s \cos \mu_s \sin \mu \cos \beta \tag{10}$$

where the angles μ_s, μ, and β are the directivity angles defined in figure 4. If it is assumed that the maximum value of $\overline{(\partial F/\partial t)^2}$ occurs at the Strouhal frequency defined as follows

$$f_{st} \approx \frac{\partial}{\partial t} \approx U/\delta \tag{11}$$

where δ is the maximum thickness of the boundary layer along the cylinder, the fluctuating dipole force can be approximated by the following expressions:

$$\overline{\left(\frac{\partial F}{\partial t}\right)^2} \approx f^2 \rho^2 U^4 A_c \approx \rho^2 U^6 \delta^2 \tag{12}$$

where $A_c \approx \delta^2$ is the dipole correlation area. Substituting equations (11) and (12) into equation (9) yields the following expression for the noise radiated from a point dipole:

$$\overline{P_g^2} \approx \frac{\rho^2 U^6 \delta^2 D(\mu_s, \mu, \beta)}{a^2 R^2} \tag{13}$$

The parameters L and D are then introduced in such a way that the total projected area of the landing gear, A_g, equals LD. Here L and D are the characteristic length and diameter, respectively, of the cylinders shown in figure 3(b). Since equation (13) represents the sound radiated from a single eddy of volume proportional to δ^3, the total sound radiated from the spanwise distribution of eddies is assumed to be proportional to L/δ. Thus, multiplying equation (13) by L/δ yields the following equation:

$$\overline{P_g^2} \approx \frac{\rho^2 U^6 L \delta D(\mu, \mu_s, \beta)}{a^2 R^2} \tag{14}$$

Again, from reference 9, $\delta \approx DC_{Dg}$ where C_{Dg} is the drag coefficient of the landing gear. Since C_{Dg} data are generally available only for the entire landing gear structure, the model assumes all of the landing gear noise to be generated from either the cylinder representing the strut or the cylinder representing the wheels. Substituting $\delta \approx DC_{Dg}$ into equation (14) and using LD = Ag yields the following expression:

$$\overline{P_g^2} \approx \frac{\rho^2 U^6 C_{Dg} A_g D(\mu, \mu_s, \beta)}{a^2 R^2} \tag{15}$$

Defining an incremental drag coefficient, ΔC_{Dg}, for the landing gear as follows

$$\Delta C_{D_g} = C_{D_g} \frac{A_g}{S_w}$$

and substituting it into equation (15) yields the following expression:

$$\overline{P_g^2} \approx \frac{K_g \rho^2 U^6 \Delta C_{Dg} S_w D(\mu, \mu_s, \beta)}{a^2 R^2} \tag{16}$$

where K_g represents the average of the variation of the point dipole distribution along the gear. The maximum overall sound pressure level for landing gear noise is as follows:

$$OASPL_g = 10 \log\left[\frac{K_g \rho^2 U^6 \Delta C_{Dg} S_w D(\mu, \mu_s, \beta)}{a^2 R^2 \overline{P_{ref}^2}}\right] \quad (17)$$

This derivation does not include possible noise generated by the impingement of the landing gear wake upon the wing flaps.

Combining equations (8) and (17) yields the final form of the airframe prediction model for the maximum overall sound pressure level. This equation is as follows:

$$OASPL = 10 \log\left[\frac{K_w C_{Dw} \rho^2 U^{4.8} S_w \cos^2(\Theta/2) \sin\phi \cos^2\psi}{aR^2(\bar{c}/\nu)^{0.2} \overline{P_{ref}^2}} + \frac{K_g \rho^2 U^6 \Delta C_{Dg} S_w D(\mu, \mu_s, \beta)}{a^2 R^2 \overline{P_{ref}^2}}\right] \quad (18)$$

For the flaps-down configuration, K_{wf} can be substituted for K_w.

Evaluation of Empirical Constants

The derivation of equation (18) assumes that the parameters K_w, K_{wf}, and K_g are constant independent of such flight conditions as airplane configuration, weight, and speed. The validity of the model was verified indirectly by using flyover noise test data to calculate the values of K_w, K_{wf}, and K_g to determine if they were indeed constant. To determine the various parameter values, the following values must be known: the component drag coefficients, wing area (S_w), wing mean aerodynamic chord ($\bar{c}$), aircraft speed (U), air density (ρ), speed of sound (a), and kinematic viscosity (ν).

The noise data were divided according to the three aircraft configurations, the first corresponding to flaps and landing gear retracted, the second to flaps extended but landing gear up, and the third to flaps extended and landing gear down (full landing configuration). For the first two configurations, the dominant noise mechanism was assumed to be the diffracted trailing-edge quadrupoles at the wing trailing

edge (for the first configuration) or the flap trailing edge (for the second configuration). For these configurations, the constant K_g equals zero in equation (18). For the third configuration, both diffracted trailing-edge quadrupoles and point dipole acoustic sources contribute to the OASPL.

The flyover noise data were obtained from three commercial jet aircraft—the Lockheed JetStar, Convair 990, and Boeing 747 aircraft. Details of the measurement program are given in references 6 and 7. Only maximum OASPL flyover noise data were analyzed. As shown in figure 2, the directivity angles were $\theta \approx 270°$ and $\varphi \approx 90°$. The aircraft parameters required for the use of equation (18) are summarized in table 1.

The aircraft was assumed to be in equilibrium during the flyover. The equations governing the aircraft motion (assuming zero acceleration and negligible thrust from the engines) are as follows:

$$W \sin \gamma = D = C_D q S_w \tag{19}$$

$$W \cos \gamma = L = C_L q S_w \tag{20}$$

where q is the dynamic pressure, $1/2\rho U^2$, and γ is the aircraft glide slope angle relative to the horizon. Equations (19) and (20) contain the three unknowns γ, C_D, and C_L. Their solution requires that either γ be specified from flight test measurements or that the relationship between the aircraft's lift and drag coefficients (the drag polar) be specified. The drag polar was used to solve for C_D because it is usually more accurate than flight test measurements of γ. In general, curve fits of C_D versus C_L take the following form:

$$C_D = C_{D_0} + K_1 (C_L)^2 + K_2 (C_L)^4 \tag{21}$$

where C_{D_0} is the value of C_D at $C_L = 0$ and K_1 and K_2 are known constants. Replacing C_D and C_L in equation (21) by the respective values from equations (19) and (20) yields the following expression:

$$C_W \sin \gamma = C_{D_0} + K_1 (C_W \cos \gamma)^2 + K_2 (C_W \cos \gamma)^4 \tag{22}$$

where $C_W = W/qS_w$. With W and U (hence q) specified from the test data, equation (22) is solved for γ. The value of C_D follows immediately from equation (19).

The results of applying this procedure to the three aircraft are summarized in tables 2(a), 2(b), and 2(c), which correspond to the first, second, and third configurations, respectively, as described above. For convenience, the results shown in tables 2(a) to 2(c) are summarized in figures 5(a) to 5(c).

Figures 5(a) to 5(c) were derived as follows. Given the aircraft weight and speed, C_D was calculated from the aircraft drag polar. Ideally, for the clean wing configuration, the drag coefficient for the wing only (including the vertical and horizontal empennage) should be used in calculating C_{Dw}. However, only the drag coefficient for the entire aircraft was available, including the contribution from the fuselage and other structural elements. Thus, drag from the fuselage and other parts of the airplane was included in the calculation. The errors associated with including the fuselage drag are not thought to be particularly large because of the high values of induced wing drag experienced during the landing maneuver. (No errors were introduced in the calculated landing gear drag coefficient, because this information was readily available.)

Nine test cases from table 2(a) (and fig. 5(a)) were analyzed for all three aircraft. The measured flight test speeds ranged from 97 meters per second to 187 meters per second. The nine values of 10 log K_w (which averaged -29.2 dB) showed no dependence on aircraft configuration, weight, or speed, validating equation (8).

Only three maximum OASPL flight test measurements were available with the wing trailing-edge flaps extended but the landing gear retracted (the second configuration) (table 2(b), fig. 5(b)). Despite the different flap deflections (50° for the JetStar airplane, 36° for the Convair 990 airplane, and 25° for the Boeing 747 airplane), the three values of 10 log K_{wf} differed by less than 1 decibel from their average value (-24.5 dB). An immediate (although admittedly preliminary) conclusion that can be drawn from this analysis is that the effect of deflecting the flaps is to increase the maximum aircraft airframe OASPL by the following amount:

$$\Delta OASPL_{max} = 10 \log \left(\frac{K_{wf} C_{Df}}{K_w C_{Dw}} \right) \tag{23}$$

$$\approx 5.1 + 10 \log \left(C_{Df} / C_{Dw} \right)$$

In deriving equation (23), the average values of the wing constants K_w and K_{wf}, which are shown in figures 5(a) and 5(b), respectively, were used.

In total, seven test cases were available to estimate the contribution to the OASPL of the landing gear. Four test cases were from the JetStar airplane, one was from the Convair 990 airplane, and two were from the Boeing 747 aircraft. The results are shown in table 2(c) and figure 5(c), where the average value of

10 log K_g is -32.9 decibels. In light of the large differences in the size and geometry of the landing gear of the aircraft, the parameter 10 log K_g is reasonably constant.

ANALYSIS OF SPECTRAL DATA

The success of equation (8) in predicting maximum OASPL for the clean configuration prompts its immediate application to the normalization of one-third OBSPL data. Figures 6 and 7 demonstrate the usefulness of this normalization. As shown in figure 7, the clean configuration JetStar one-third OBSPL data shown in figure 6 collapse into a single correlation curve at frequencies in excess of 500 hertz. This suggests that the one-third octave band center frequency (OBCF) of 1250 hertz characterizes the Ffowcs Williams and Hall diffracted quadrupole trailing-edge type of Strouhal frequency. The correlation of the data for frequencies less than 500 hertz, which is not as good as at the higher frequencies, suggests that this part of the spectrum is radiated by a mechanism other than trailing-edge noise. This is consistent with the derivation of equation (8), which requires the wavelength of interest to be much shorter than the local chord. At the one-third OBCF of 1250 hertz, the wavelength is approximately 0.27 meter, considerably shorter than the 3.04-meter JetStar wing mean chord length. For frequencies less than 500 hertz, the sound wavelengths are on the order of the mean chord, in violation of the Ffowcs Williams and Hall theory.

Figures 6 and 7 show that the frequency for the maximum one-third OBSPL is independent of aircraft speed. Further, figure 8 shows that the one-third OBCF corresponding to the maximum sound pressure level for the clean wing data of the JetStar, Convair 990, and Boeing 747 aircraft is also virtually independent of aircraft geometry and speed. Although the reason for the insensitivity of the variation of peak frequency to aircraft speed and geometry is not known, the following observations may be made. In deriving their model, Ffowcs Williams and Hall divided the turbulent eddy structure at the surface trailing-edge region into two categories, one corresponding to $K\delta \gg 1$ and the other to $K\delta \ll 1$. They showed that only the eddies that satisfied the constraint that $K\delta \ll 1$ contributed significantly to edge noise. It follows that only very small, high frequency eddies are scattered by the trailing edge. Since these eddies are close to the surface, their behavior may be controlled more by local trailing-edge shear forces than by global airfoil chord-based Reynolds number. The local structure of the turbulent flow field near the wing trailing edge may be relatively insensitive to variations in airfoil chord length and airplane speed (that is, Reynolds number), in accord with figures 6 to 8.

The effect on the radiated noise of extending the JetStar landing gear is shown in figure 9. The data were normalized by using equation (8) to compare them with the average clean wing data as shown. Figure 9 shows that the effects of deploying the landing gear are to increase the level of the clean wing peak one-third OBSPL frequency (1250 Hz) by roughly 8 decibels and to establish a secondary peak in the one-third OBSPL in the lower frequency range extending from 160 hertz to 250 hertz.

The reason for the increase in the sound pressure level at a one-third OBCF of 1250 hertz is not clear. It may be due to the interaction of the landing gear wake and the wing trailing edge. The reason for the secondary peak at a frequency of approximately 200 hertz is not fully understood. For example, if it is assumed that the low frequency peak is generated by the landing gear structure, a characteristic dimension, D_{ch}, in meters, is as follows:

$$D_{ch} = \frac{S_c V}{f} = \frac{(0.21)(93.6)}{200} = 0.098$$

where a value of 0.21 is obtained for S_c (ref. 9, p. 31). The 9.8-centimeter dimension cannot be clearly identified with any part of the JetStar landing gear (fig. 10). The JetStar landing gear is simple compared to the more complex gear of bigger aircraft.

The data in the remaining figures have been normalized by using equation (8) with the clean wing drag coefficient used for all configurations, so that the effects of the landing gear and the flaps can be shown.

Figure 11 shows the effects of flap deflection on the spectral data for the JetStar airplane. The data for the gear-down 0° flap deflection from figure 9 are similar to the data for the gear-up 50° flap deflection, except at the low frequencies, where the flaps cause an increase of about 5 decibels. The data for the gear-down 50° flap deflection show almost no change from the data for the gear-up 50° flap deflection.

Figure 12 shows the effect of landing gear and flap deflection on the one-third OBSPL data for the Convair 990 airplane. The effect of deflecting the flaps is to increase the one-third OBSPL by 6 decibels to 8 decibels for frequencies below approximately 1000 hertz. When the landing gear are down with the flaps deflected, an additional 2 decibels to 3 decibels of noise is generated at frequencies below 500 hertz.

The Boeing 747 gear and flap data are shown in figure 13. Extending the landing gear with no flap deflection results in an increase in one-third OBSPL of 8 decibels to 10 decibels over the clean configuration up to approximately 2000 hertz and about 5 decibels above 2000 hertz. A photograph of the Boeing 747 main landing gear is shown in figure 14. The gear, struts, and doors are much more complex than those of the JetStar airplane. Extending the flaps 25° with the landing gear up results in a larger increase in one-third OBSPL below 500 hertz, and a smaller increase above 500 hertz. The gear-down flaps-extended data appear to be approximately equal to the sum of the gear-only and flap-only data.

Summarizing the effects of extending the landing gear and deflecting the flaps, two preliminary conclusions can be drawn for the three aircraft. First, if the flaps are deflected, little increase in OASPL or in one-third OBSPL is caused by extending the landing gear. Also, with the landing gear extended, the effect of deflecting the flaps is to increase the one-third OBSPL for frequencies below approximately 500 hertz.

A summary of the one-third OBSPL data with the flaps deflected for the three airplanes tested is shown in figure 15. No particular characteristic frequency is evident, with the spectral shape generally flat from 100 hertz to 2000 hertz.

The gear- and flaps-down data for the three airplanes are summarized in figure 16. As in figure 15, the spectra tend to be relatively flat. At frequencies below 2000 hertz, the normalized data for the three airplanes agree very well. The important point in figures 15 and 16 is that the spectra correlate well using the theory of Ffowcs Williams and Hall despite the differences in size of the three aircraft.

CONCLUSIONS

Despite a relatively small data base and large variations in airplane geometry and size, the correlation of the maximum overall sound pressure level flyover noise data found in this study is encouraging. The following conclusions regarding the characteristics of airframe-generated noise have been reached:

1. With flaps and landing gear retracted, maximum overall flyover airframe-generated noise has been successfully correlated using the Ffowcs Williams and Hall trailing-edge diffracted quadrupole sound theory.

2. With flaps extended, Ffowcs Williams and Hall's theory also correlates successfully with the resulting airframe noise. This conclusion is tentative, however, in view of the extremely limited data base.

3. Landing gear noise has been correlated using point acoustic dipole sources. Again, this conclusion is tentative because of the extremely limited data base.

4. The use of the clean wing Ffowcs Williams and Hall theory appears to be a good way to normalize data obtained with the landing gear extended and the flaps deflected. Using this approach, the flight data show that if the flaps are deflected, extending the landing gear causes little increase in noise, and conversely, that if the landing gear is extended, the effect of deflecting the flaps is to increase noise at frequencies below approximately 500 hertz.

The insight gained from this study suggests that further work on evaluation of the model should be done. It would be of value to extend the model to predict time histories of flyover noise to verify the predicted directivity angles. It would also be of value to conduct diagnostic tests in a wind tunnel of the noise radiation characteristics of airplane wings and flaps to verify directly the Ffowcs Williams and Hall theory.

Dryden Flight Research Center
National Aeronautics and Space Administration
Edwards, Calif., September 22, 1976

REFERENCES

1. Civil Aviation Research and Development Policy Study. DOT TST-10-4, NASA SP-265, Mar. 1971.

2. Curle, N.: The influence of solid boundaries upon aerodynamic sound. Proc. Roy. Soc. (London), ser. A, vol. 231, 1955, pp. 505-514.

3. Ffowcs Williams, J. E.; and Hall, L. H.: Aerodynamic Sound Generation by Turbulent Flow in the Vicinity of a Scattering Half Plane. J. Fluid Mech., vol. 40, Mar. 9, 1970, pp. 657-670.

4. Lighthill, M. J.: On sound generated aerodynamically. II. Turbulence as a source of sound. Proc. Roy. Soc. (London), ser. A, vol. 222, 1954, pp. 1-32.

5. Fink, M. R.: Experimental Evaluation of Trailing Edge and Incidence Fluctuation Noise Theories. AIAA Paper 75-206, Jan. 1975.

6. Lasagna, P. L.; and Putnam, T. W.: Preliminary Measurements of Aircraft Aerodynamic Noise. AIAA Paper 74-572, June 1974.

7. Putnam, T. W.; Lasagna, P. L.; and White, K. C.: Measurements and Analysis of Aircraft Airframe Noise. AIAA Paper 75-510, Mar. 1975.

8. Healy, Gerald J.: Measurement and Analysis of Aircraft Far-Field Aerodynamic Noise. NASA CR-2377, Dec. 1974.

9. Schlichting, Hermann: Boundary Layer Theory. Fourth ed., McGraw-Hill Book Co., Inc., 1960.

10. Powell, Alan: Aerodynamic Noise and the Plane Boundary. J. Acoust. Soc. Am., vol. 32, no. 8, Aug. 1960, pp. 982-990.

11. Revell, J. D.: On the calculation of aerodynamic noise generated by large aircraft at landing approach. J. Acoust. Soc. Am., vol. 55, Suppl., Spr. 1974, p. S73.

12. Hardin, Jay C.; Fratello, David J.; Hayden, Richard E.; Kadman, Yoran; and Africk, Steven: Prediction of Airframe Noise. NASA TN D-7821, Feb. 1975.

Table 1. Airplane wing geometrical parameters

Airplane	S_w, m^2	$\bar{c}$, m	ψ, deg
JetStar	50.4	3.04	30.0
Convair 990	209.0	5.47	35.0
Boeing 747	511.0	8.32	37.5

Table 2. Evaluation of constants for three aircraft configurations

(a) Evaluation of constant for clean wing

Airplane	W, N	U, m/sec	Measured OASPL, dB	10 log K_w, dB
JetStar	161,018	128.6	84.5	-29.3
	158,349	155.4	87.1	-30.0
	155,680	177.5	90.2	-29.4
	151,232	182.7	90.4	-29.7
	148,118	187.8	91.0	-29.6
Convair 990	809,542	161.0	93.9	-29.3
	698,340	97.2	86.1	-28.4
Boeing 747	2,233,000	139.5	95.0	-28.5
	2,228,000	120.2	92.8	-28.6

Table 2. Continued

(b) Evaluation of constant for wing with flaps extended

Airplane	Flap setting, deg	W, N	U, m/sec	Measured OASPL, dB	10 log K_{wf}, dB
JetStar	50	140,272	87.5	87.3	-25.4
Convair 990	36	738,000	97.7	92.8	-25.0
Boeing 747	25	2,255,000	105.4	99.0	-23.3

Table 2. Concluded

(c) Evaluation of constant for landing gear

Airplane	Flap setting, deg	W, N	U, m/sec	Measured OASPL, dB	10 log K_g, dB
JetStar	0	137,937	93.6	87.3	-32.0
	0	135,157	103.4	88.9	-33.7
	0	131,154	104.9	88.4	-34.8
	50	132,043	81.2	86.8	-32.7
Convair 990	36	749,488	82.3	92.7	-31.6
Boeing 747	25	2,277,000	104.8	101.8	-32.4
	25	2,211,000	114.5	101.1	-33.4

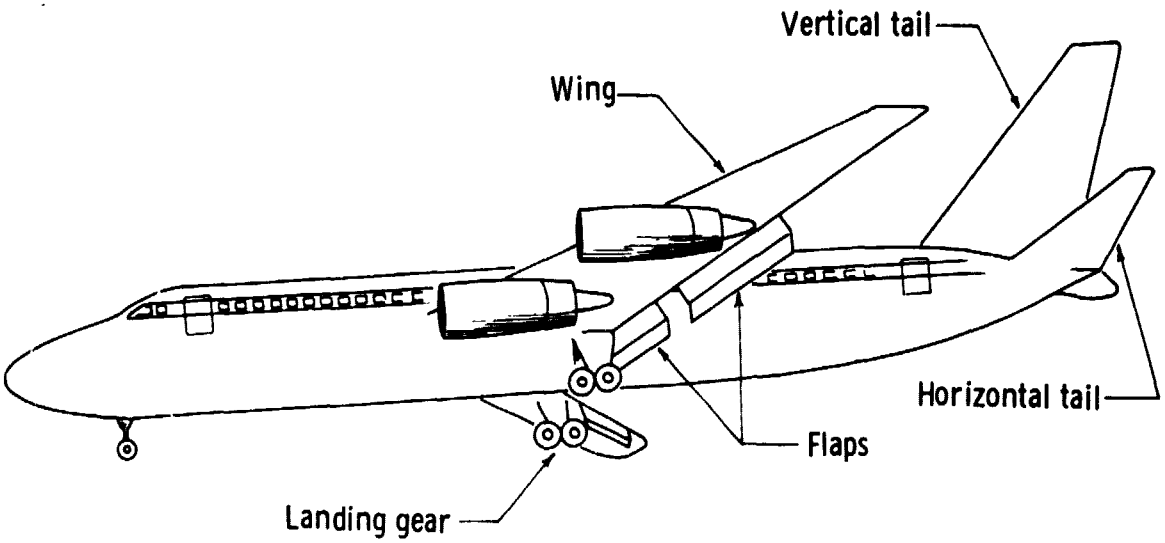

Figure 1. Sources of airframe noise.

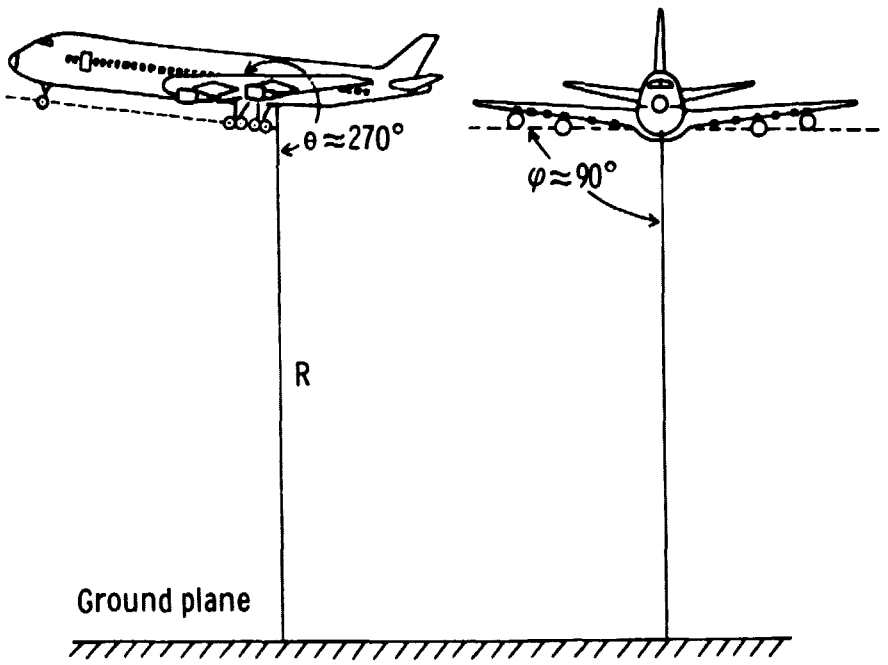

Figure 2. Directivity angles for quadrupole trailing-edge diffracted noise sources.

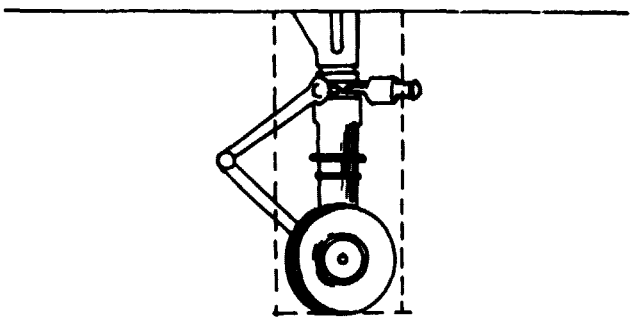

(a) Schematic of cylinder formed by single strut.

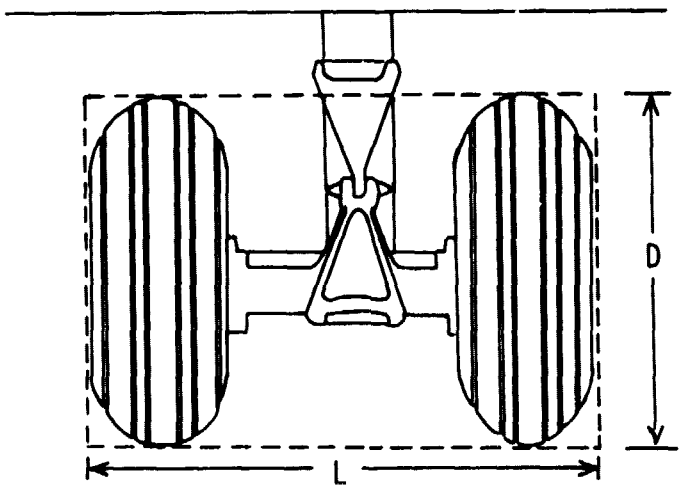

(b) Schematic of cylinder formed by wheels.

Figure 3. Idealized representation of landing gear.

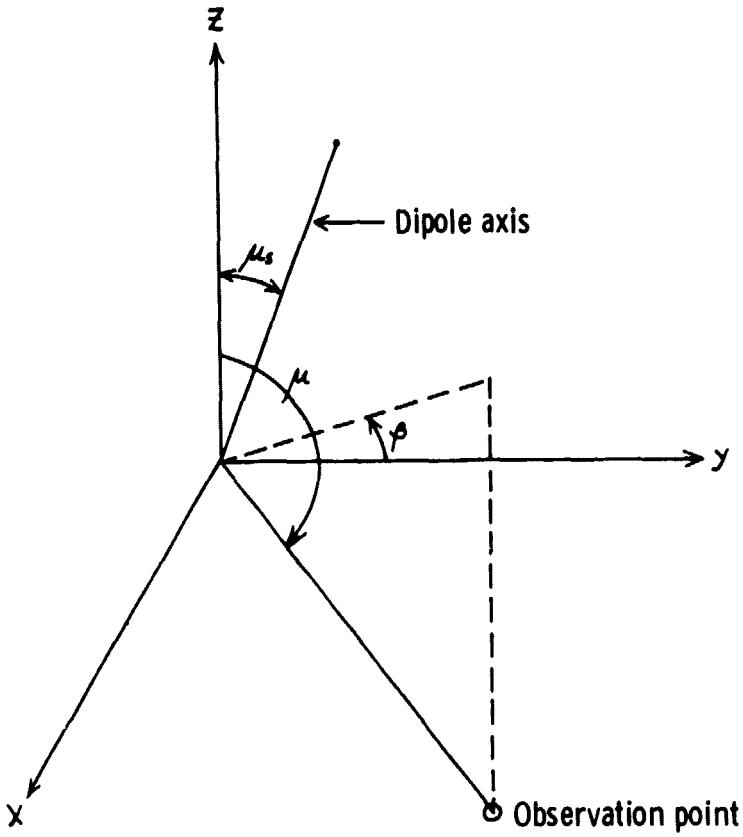

Figure 4. Definition of directivity angles for dipole sources.

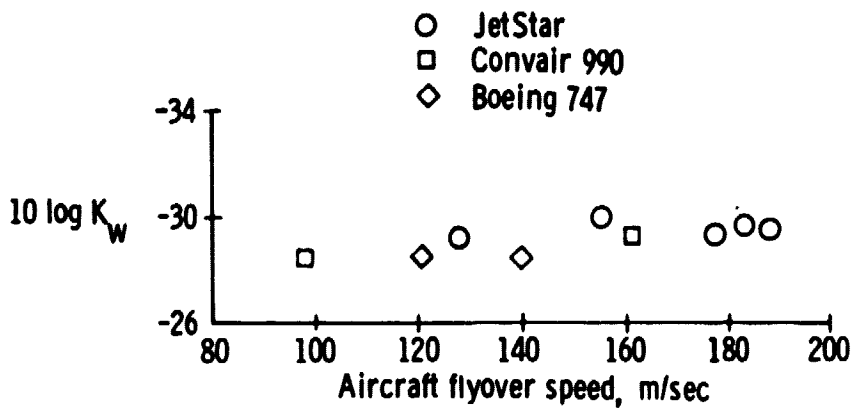

(a) Flaps retracted, landing gear up.

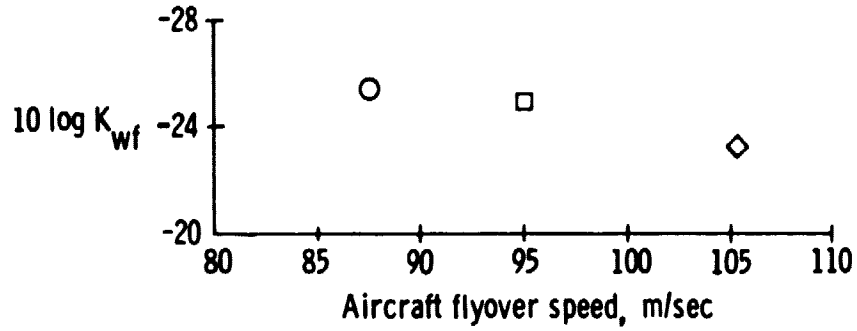

(b) Flaps extended, landing gear up.

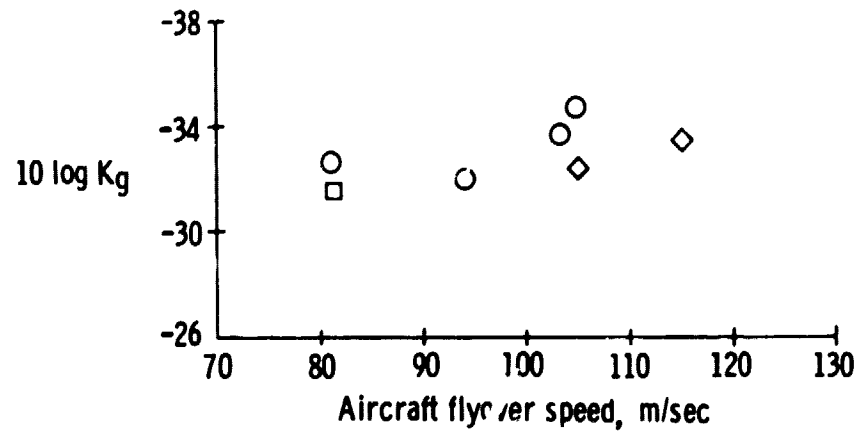

(c) Flaps extended, landing gear down.

Figure 5. Evaluation of airframe-generated noise constants.

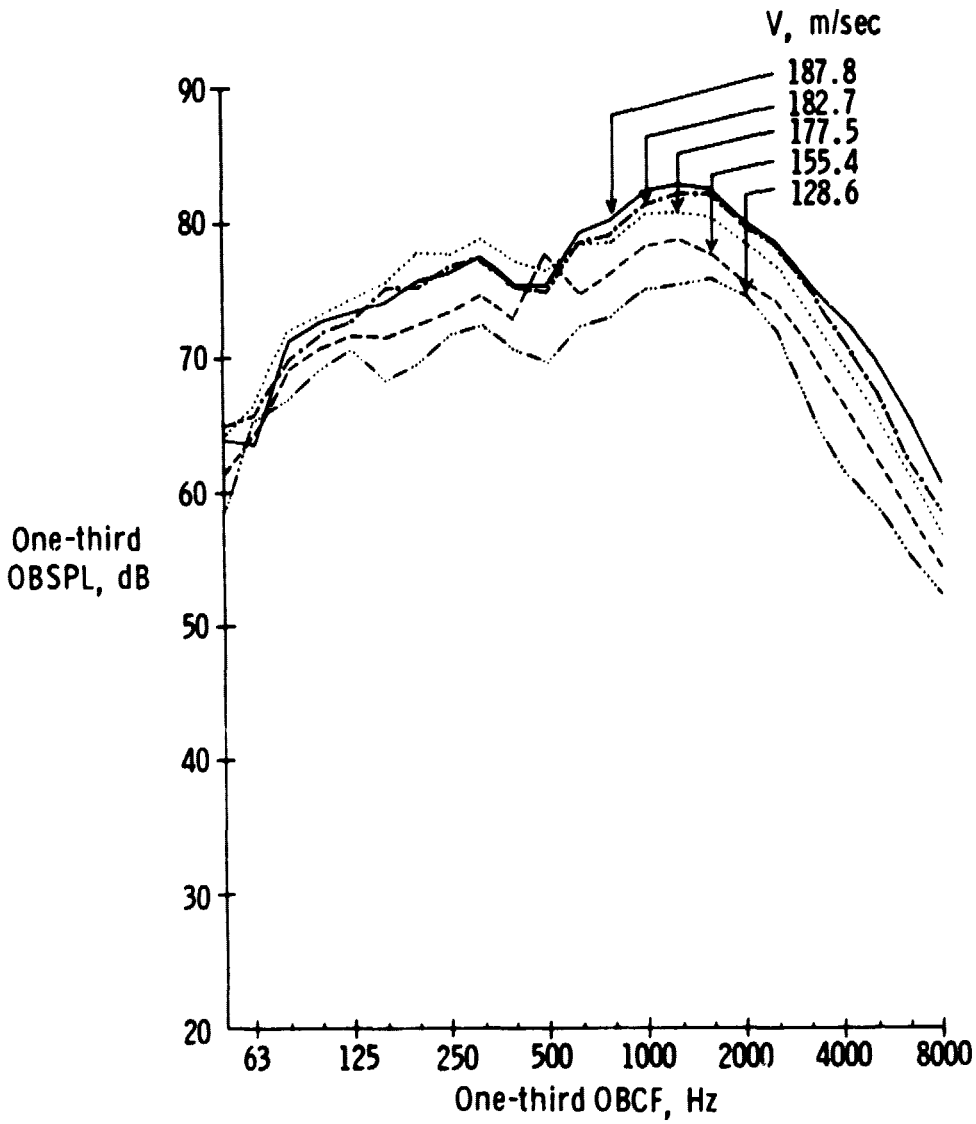

Figure 6. JetStar clean wing one-third OBSPL data.

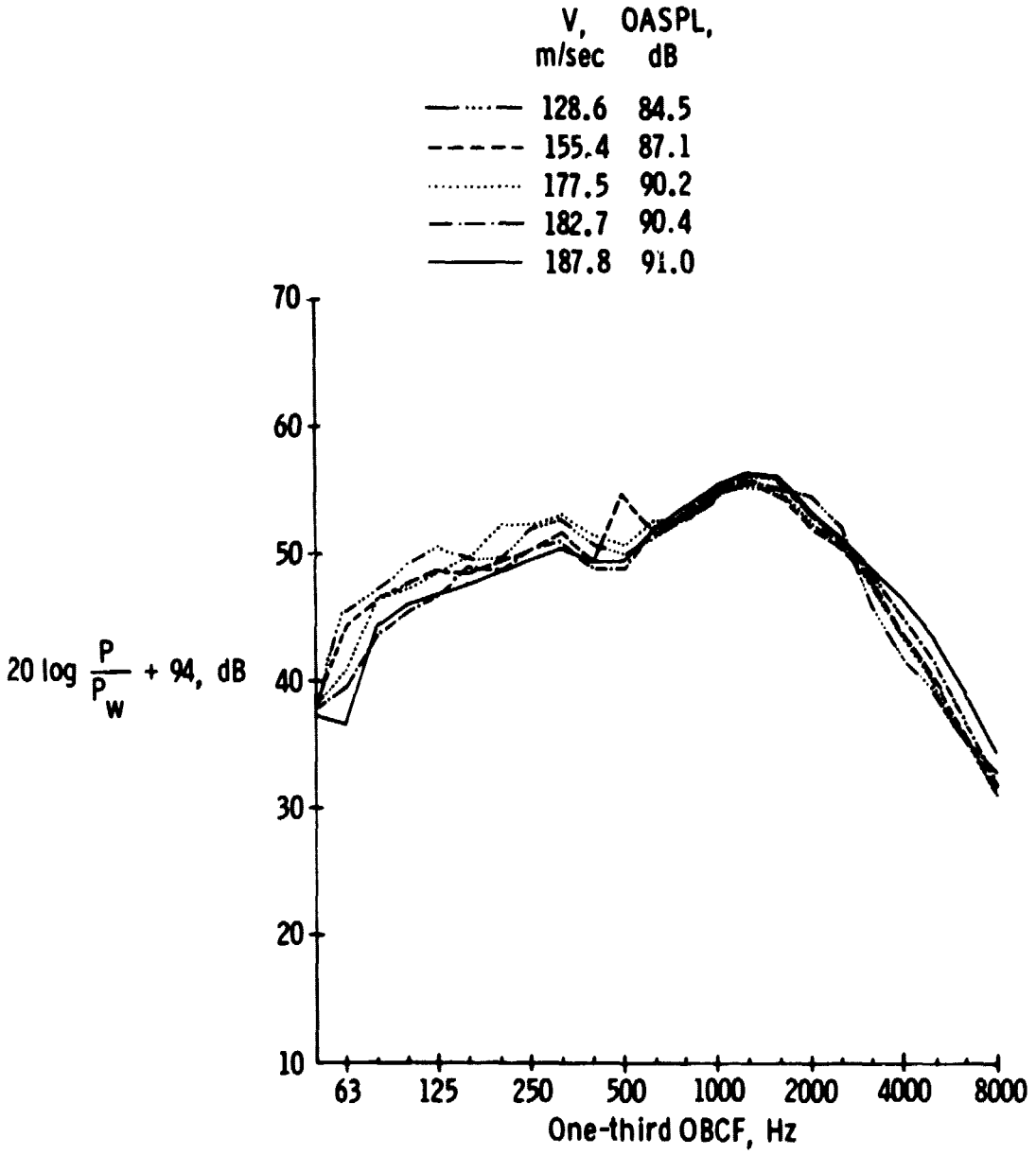

Figure 7. JetStar normalized clean wing one-third OBSPL data.

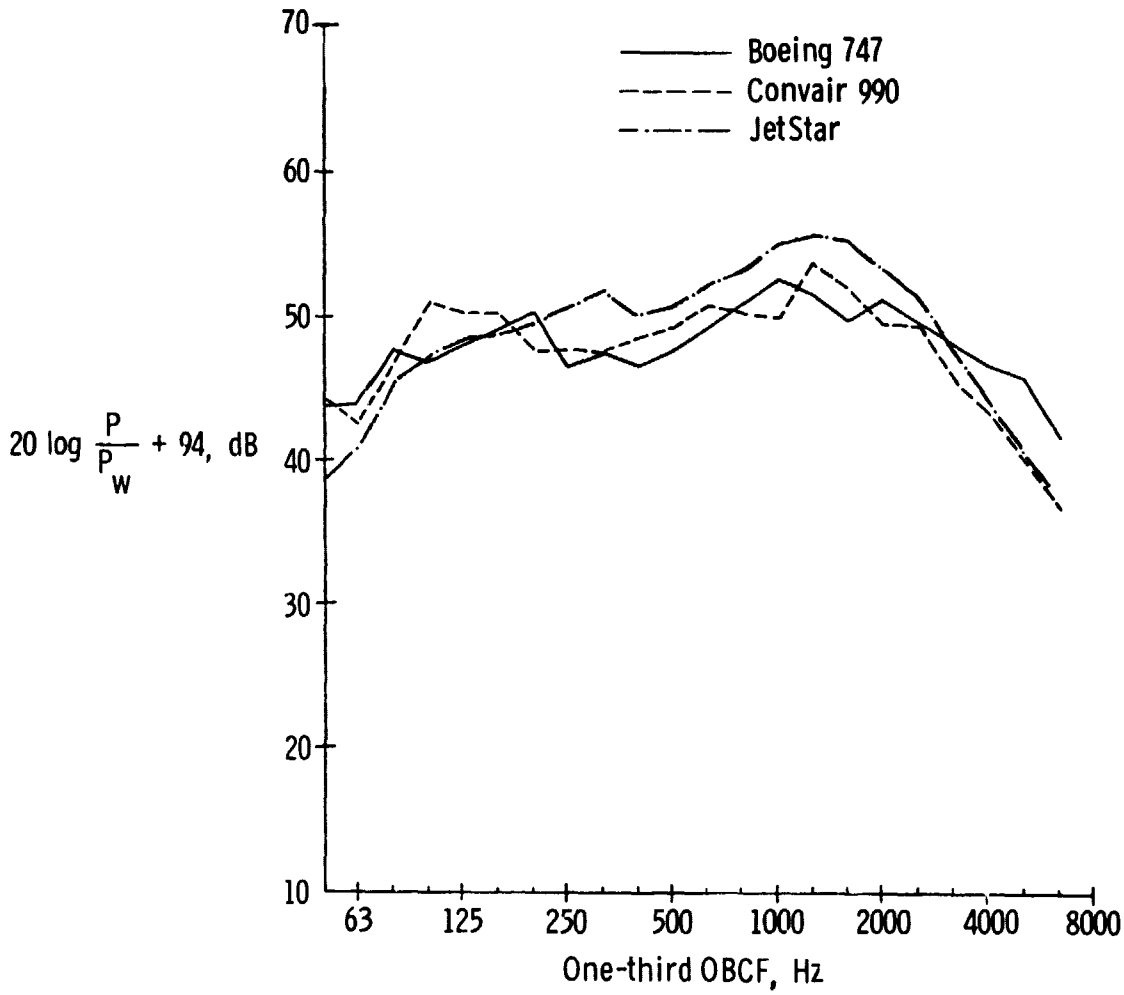

Figure 8. Comparison of airframe noise spectra for the landing gear and flaps retracted.

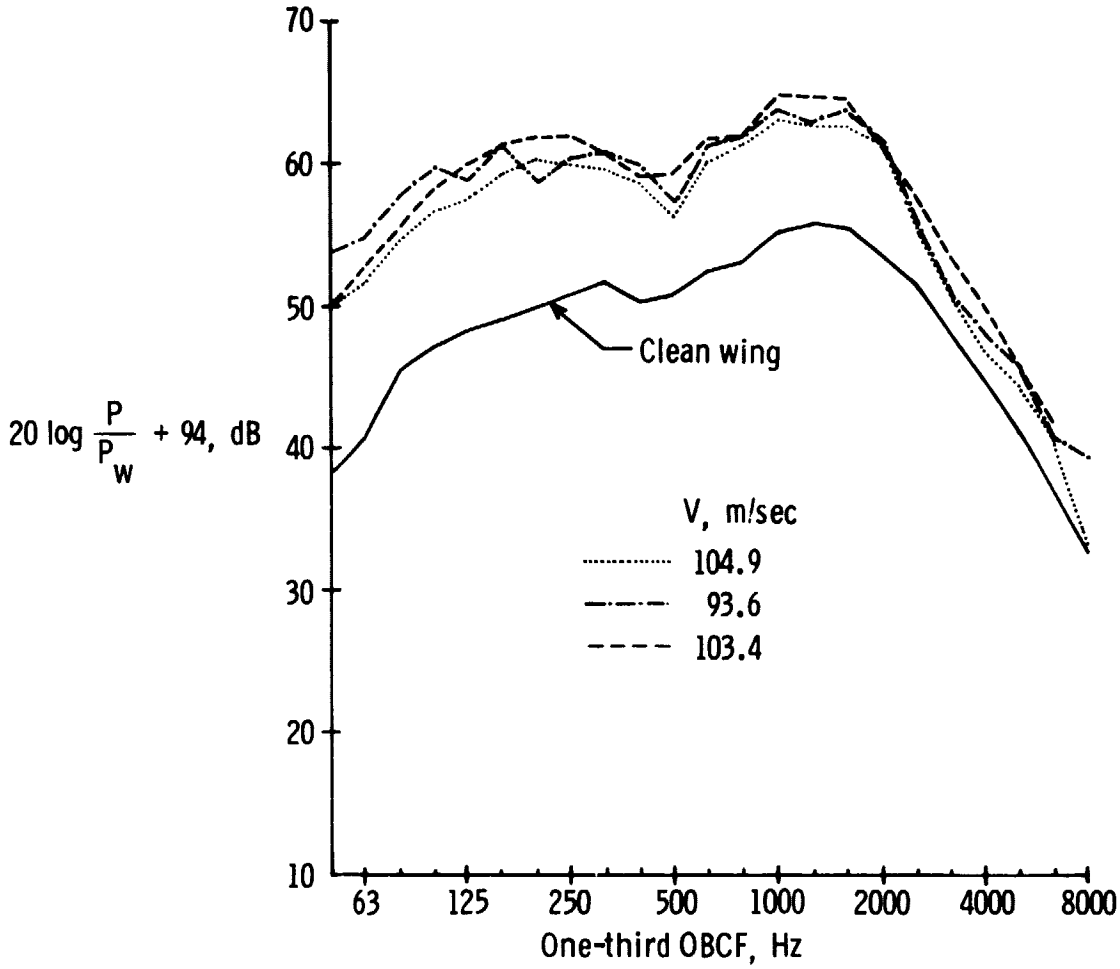

Figure 9. Effect of extending JetStar landing gear. Flaps retracted.

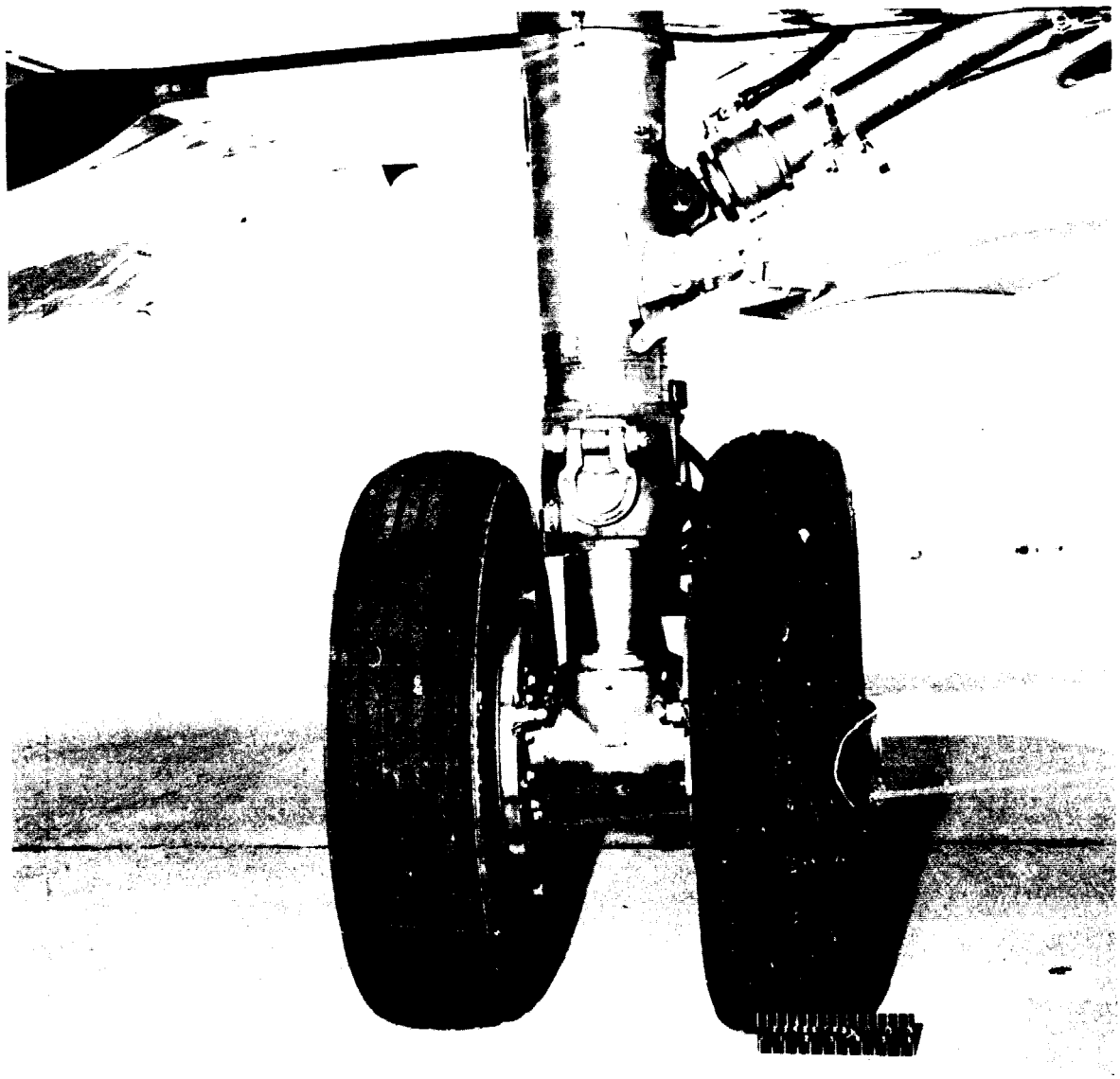

E-27519

Figure 10. JetStar main landing gear.

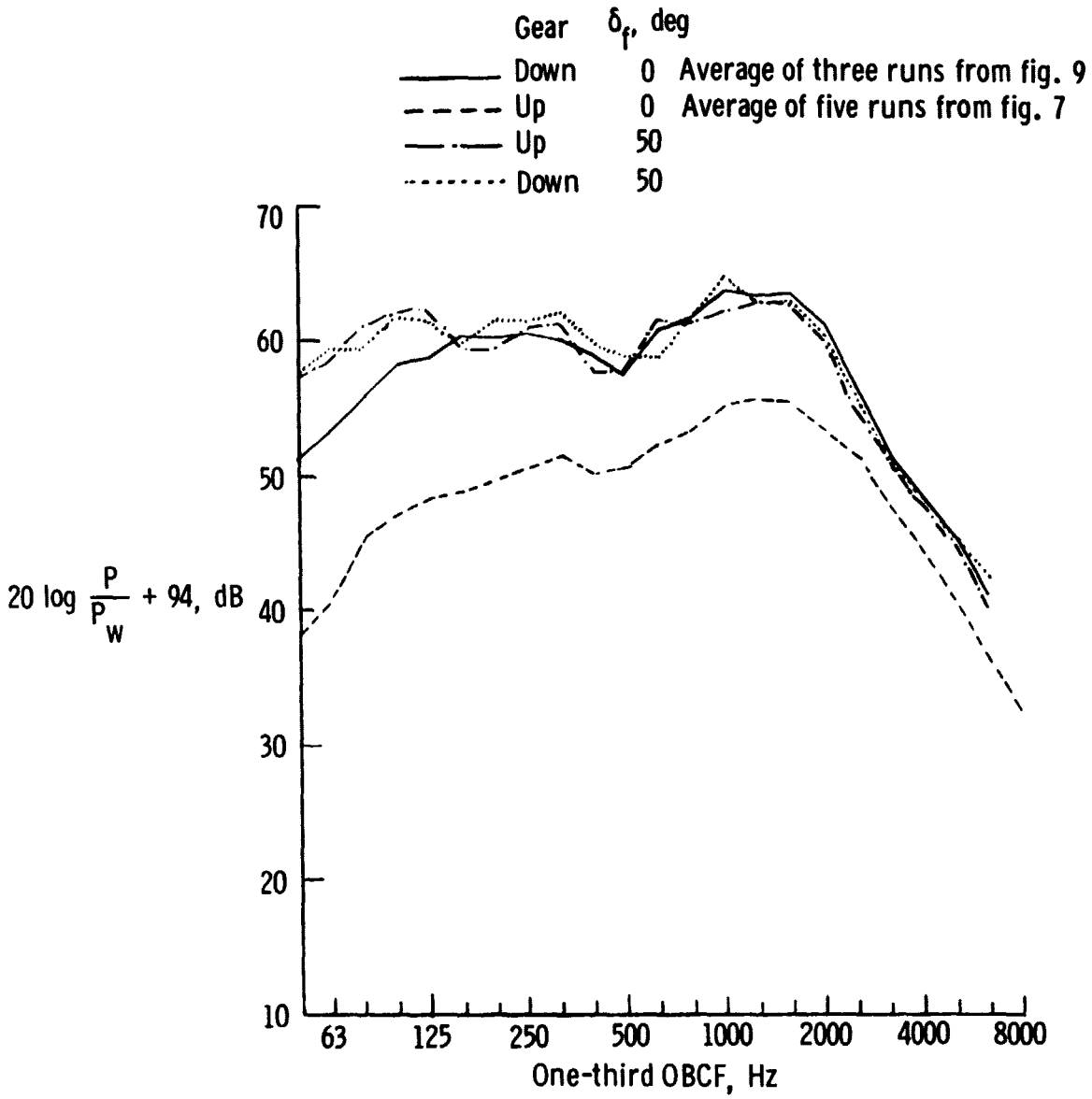

Figure 11. Effects of landing gear and flaps on airframe noise spectra for JetStar airplane.

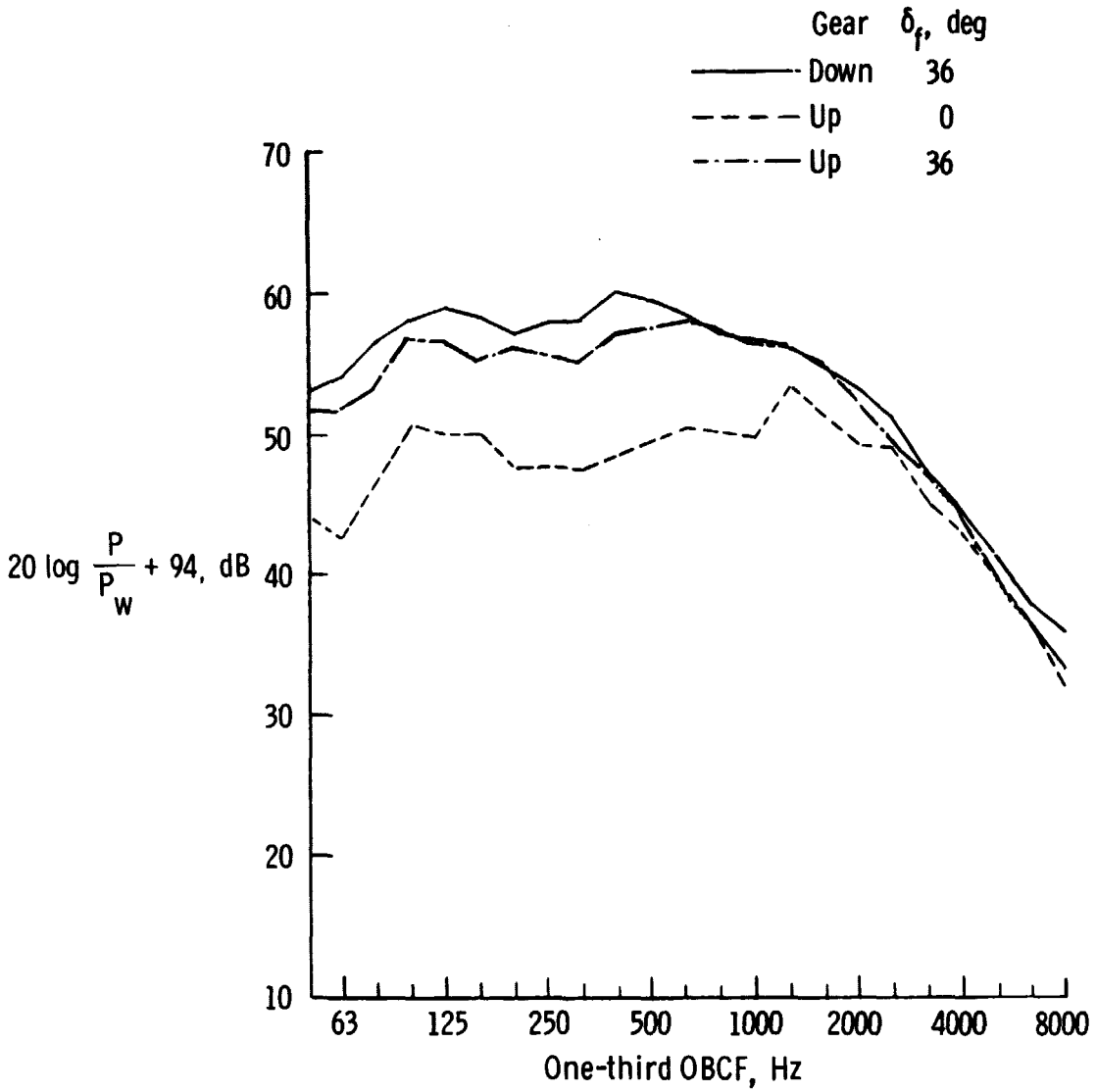

Figure 12. Effects of landing gear and flaps on airframe noise spectra for Convair 990 airplane.

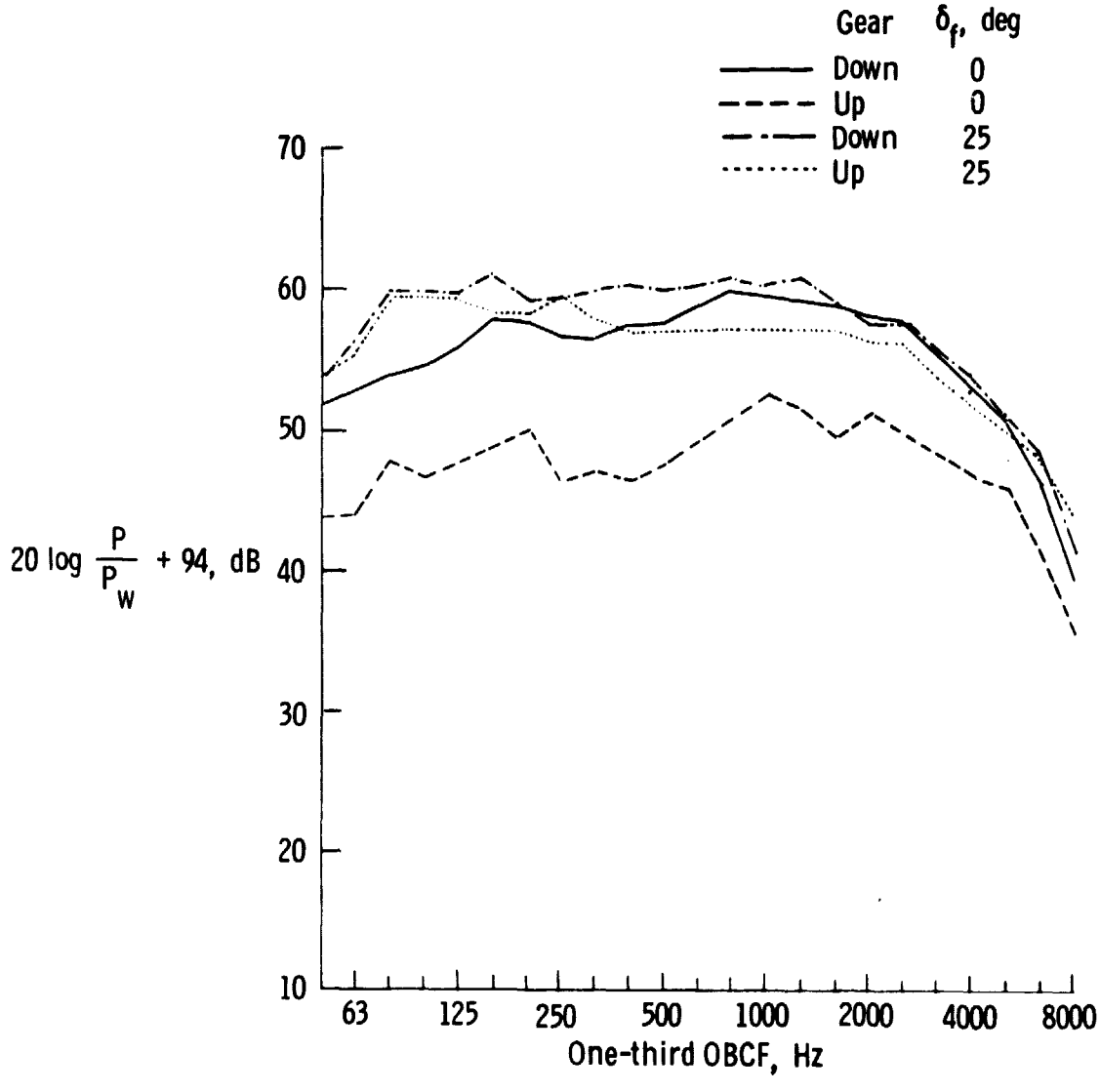

Figure 13. Effects of landing gear and flaps on airframe noise spectra for Boeing 747 airplane.

E-29229

Figure 14. Boeing 747 main landing gear.

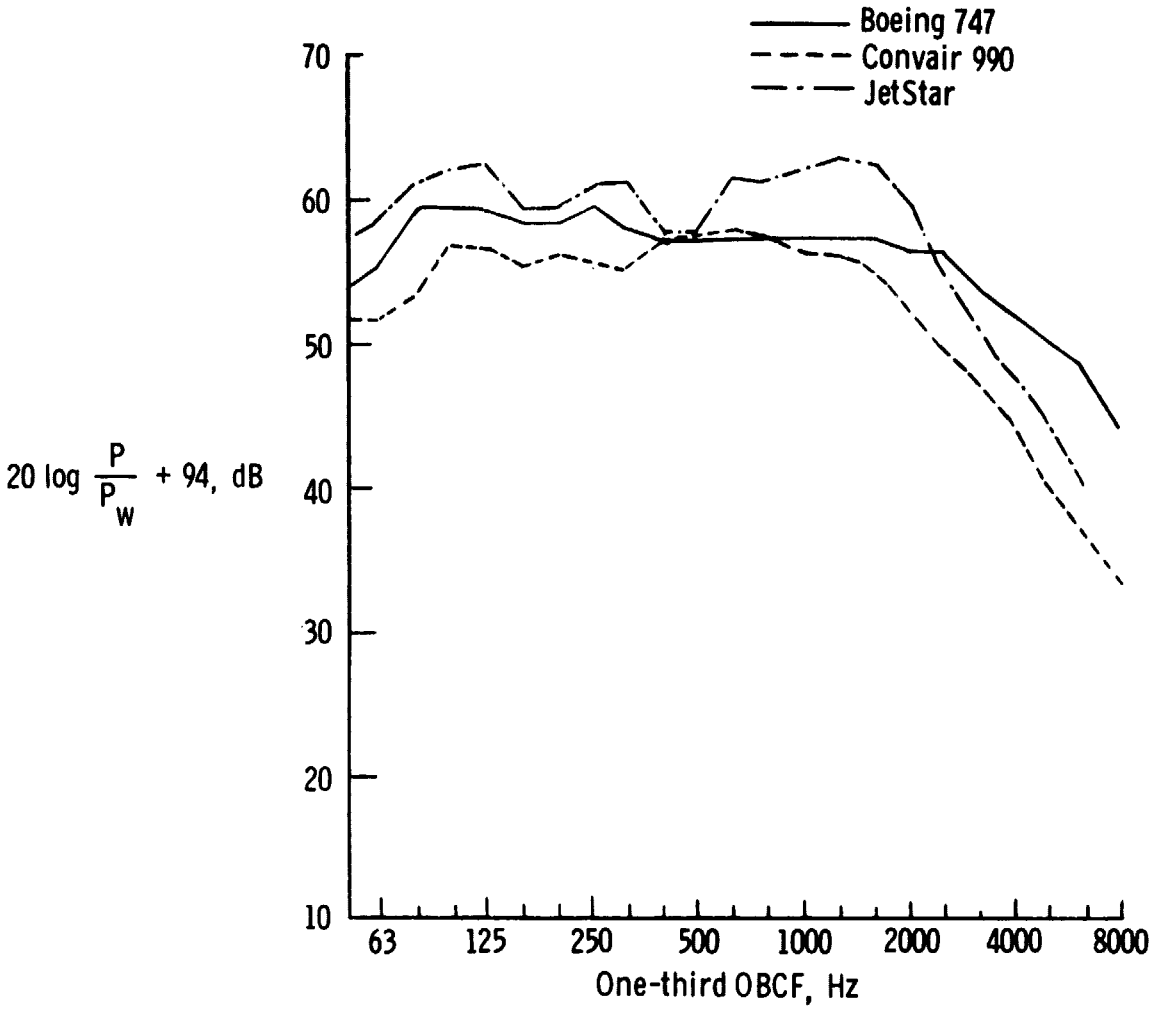

Figure 15. Comparison of airframe noise spectra for flaps extended, landing gear retracted.

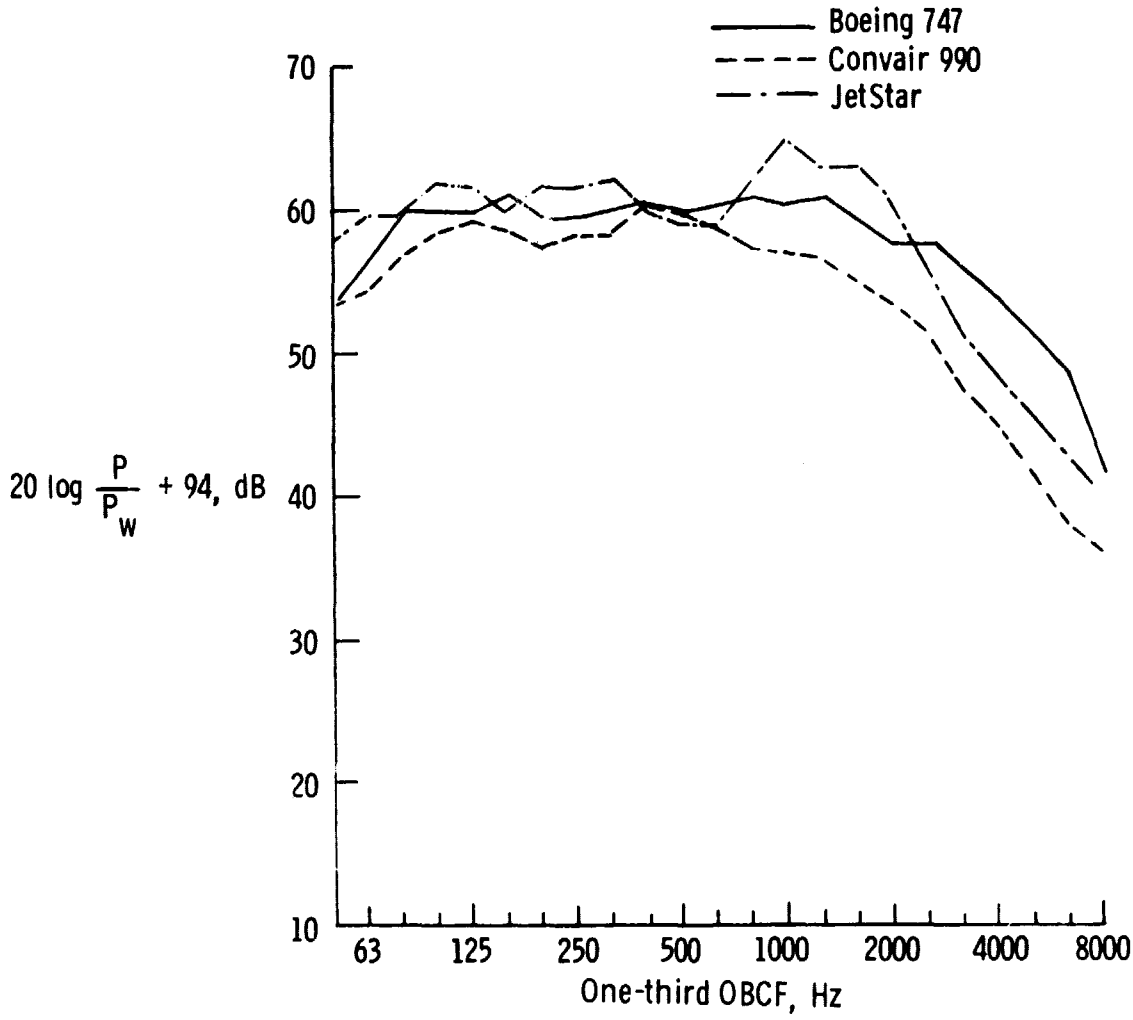

Figure 16. Comparison of airframe noise spectra for landing gear down, flaps extended.